NJC

Accepted Manuscript

This article can be cited before page numbers have been issued, to do this please use: S. Laine, C. S. Bonnet, F. K. Kálmán, Z. Garda, A. Pallier, F. Caillé, F. Suzenet, G. Tircsó and E. Toth, *New J. Chem.*, 2018, DOI: 10.1039/C8NJ00648B.

ROYAL SOCIETY OF CHEMISTRY

rsc.li/njc

View Article Online
DOI: 10.1039/C8NJ00648B

Journal Name

ARTICLE

Mn^{2+} complexes of open-chain ligands with a pyridine backbone: less donor atoms lead to higher kinetic inertness

Received 00th January 20xx,
Accepted 00th January 20xx

DOI: 10.1039/x0xx00000x

www.rsc.org/

Sophie Laine,[a] Célia S. Bonnet,[a] Ferenc K. Kálmán,[b] Zoltán Garda,[b] Agnès Pallier,[a] Fabien Caillé,[a,c] Franck Suzenet,[c] Gyula Tircsó[b *] and Éva Tóth[a *]

The kinetic inertness of Mn^{2+} complexes is an important parameter for the *in vivo* safety of potential MRI contrast agents. Rigidifying the ligand structure typically leads to reinforced kinetic inertness. In this context, we studied the Mn^{2+} complexes of three linear poly(amino carboxylate) ligands containing a pyridine moiety in their skeleton and bearing four (L^1, L^2) or three carboxylates (L^3). The thermodynamic stability constants of the complexes formed with Mn^{2+}, Ca^{2+}, Mg^{2+}, Zn^{2+} and Cu^{2+} have been determined by pH-potentiometry, ^1H relaxometry and UV/Vis spectrophotometry and are close to those of the EDTA analogues. In contrast, and despite the presence of the pyridine in the ligand backbone, the dissociation rates of the complexes are several orders of magnitude higher than that of $[Mn(EDTA)]^{2-}$, resulting from a very efficient dissociation pathway catalyzed by the direct attack of Cu^{2+} or $Cu(OH)^+$. Due to the fewer carboxylate functions, ligand L^3 is less favorable for metal-assisted dissociation and provides higher kinetic inertness for its Mn^{2+} chelate than the L^1 and L^2 analogues. The water exchange of the monohydrated MnL^3 complex has been studied in a variable temperature ^{17}O NMR study. The exchange rate is very high; k_{ex}^{298} = 2.8×10^9 s^{-1}, among the highest values reported for a Mn^{2+} complex. The NMRD profiles are typical of small molecular weight Mn^{2+} chelates (r_{1p} = 2.44 mM^{-1}s^{-1} at 25 °C and 20 MHz).

Introduction

Since the approval of $[Gd(DTPA)(H_2O)]^{2-}$ (DTPA – diethylenetriamine-*N,N,N′,N″,N″*-pentaacetic acid) in 1988 as the first contrast agent for Magnetic Resonance Imaging, Gd^{3+} complexes of poly(amino carboxylate) ligands have been extensively used in the clinics and generated important research efforts.[1] Despite the pivotal role of these imaging probes in the clinical success of MRI, recent years have witnessed a growing concern about their safety. The establishment of a causal link between nephrogenic systemic fibrosis (NSF)[2] and Gd-injections or the recent reports on detectable amounts of Gd in the brain[3] have alerted the medical community and showed that Gd complexes should be used with caution in certain situations, like in patients with impaired renal function. Even if Gd-based agents can be in general considered as harmless, these concerns have promoted intensive research to identify safer alternatives. In this respect, Mn^{2+} complexes attracted most attention.[4-9] Manganese is a biogenic element and its 5 unpaired electrons as well as its slow electronic relaxation make Mn^{2+} the most obvious candidate to replace Gd^{3+} in MRI contrast agent applications. Although manganese is naturally present in the body, the high quantities of contrast agents typically injected for MR imaging imply that the Mn^{2+} complexes should be thermodynamically stable and kinetically inert in order to avoid the release of larger amounts of the free metal ion which could potentially lead to toxicity. In general, the thermodynamic stability of Mn^{2+} chelates is lower than that of Gd^{3+} analogues which is primarily due to the lower charge of the Mn^{2+} ion. Moreover, given the symmetrical d^5 electronic configuration, Mn^{2+} complexes lack ligand field stabilization energy. Hence, they have lower stability than other divalent transition metal analogues (Fe^{2+}, Co^{2+}, Ni^{2+}, Cu^{2+} or Zn^{2+}). Kinetic inertness is another important factor for the *in vivo* use of metal chelates. Dissociation usually takes place *via* acid- and metal-assisted pathways, the latter referring to the direct attack of essential metal ions e.g. Cu^{2+} and Zn^{2+} on the complexes.[10] For certain complexes, Ca^{2+} may also promote the dissociation since the stability of the Ca^{2+} complex may approach that of the Mn^{2+} analogue and Ca^{2+} is highly abundant in body fluids (for the EGTA ligand for instance the difference in the stability constants is just 1-2 log units, EGTA=ethyleneglycol-bis(2-aminoethylether)-*N,N,N′,N′*-tetraacetic acid).[11] In overall, different ligand structures, both linear and macrocyclic, have been proposed for Mn^{2+} complexation, but high kinetic inertness remains difficult to achieve for Mn^{2+} complexes while keeping at least one water molecule in the inner coordination sphere.

Ligand rigidity is generally considered to promote kinetic inertness of metal complexes. For instance, the remarkably slow dissociation of $[Mn(CDTA)]^{2-}$ could be clearly related to the rigid structure of the ligand which provides a compact and preorganized coordination cavity to encapsulate the metal ion (CDTA = *trans*-1,2-

[a] Centre de Biophysique Moléculaire, CNRS, Université d´Orléans, rue Charles Sadron, 45071 Orléans, Cedex 2, France
[b] Department of Inorganic and Analytical Chemistry, Faculty of Science and Technology, University of Debrecen, Debrecen, Egyetem tér 1, H-4010, Hungary.
[c] Institut de Chimie Organique et Analytique, UMR 7311 CNRS, Université d'Orléans, rue de Chartres, 45067 Orléans, France

Electronic Supplementary Information (ESI) available: Potentiometric titration curves, pH-dependent UV/Vis spectra (Cu^{2+}/L^1) and relaxivities (Mn^{2+}/L^1), equations used for the analysis of ^{17}O NMR and NMRD data. See DOI: 10.1039/x0xx00000x

View Article Online
DOI: 10.1039/C8NJ00648B

diaminocyclohexane-*N,N,N',N'*-tetraacetic acid).[12] This study evidenced for the first time that linear ligands can also provide sufficient kinetic inertness for Mn^{2+} chelates. Caravan et al. replaced one carboxylate function of the CDTA by a pyridine to obtain the ligand PyC3A (*N*-picolyl-*N,N',N'*-trans-1,2-cyclohexylenediamine triacetate) which was shown to form a Mn^{2+} complex of comparably good stability and inertness as CDTA.[5] $[Mn(PyC3A)]^-$ was conjugated to a fibrin-specific peptide and proved promising for *in vivo* MR imaging in a rat model of arterial thrombosis.

We have previously explored pyridine-containing, open-chain poly(amino carboxylate) ligands for lanthanide complexation.[13-15] They turned to be interesting as the complexes have reasonable thermodynamic stability, the Gd^{3+} analogues contain two inner sphere water molecules thus have high proton relaxivity, and the pyridine is a good sensitizer when luminescent lanthanides, including NIR emitting ones, are complexed, despite the presence of the two hydration water molecules. Importantly, the kinetic inertness of the GdL^1 complex (Scheme 1) was found remarkable, which was related to the rigidifying effect of the pyridine in the ligand skeleton.[13] A Mn^{2+} complex formed with a 2,6-bis-aminomethyl pyridine derivative containing two piperidine rings has been also reported.[15] It had improved longitudinal relaxivity, but its kinetic inertness has not been investigated. After structural modification, this chelate has been conjugated to amphiphilic dextran micelles and suggested for vascular imaging.[16, 17]

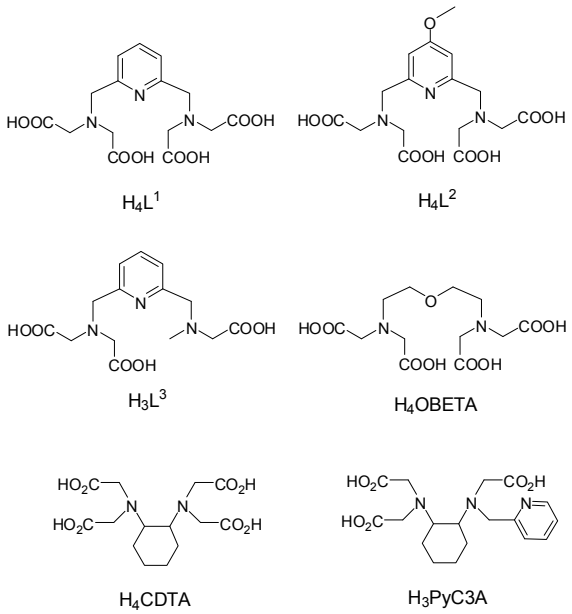

Scheme 1. Ligands discussed in the text

The objective of the present study was to investigate the influence of the pyridine in the ligand backbone of linear ligands on the thermodynamic stability and kinetic inertness of their Mn^{2+} complexes. Since the ligands H_4L^1 and H_4L^2 have seven coordinating functions, no inner sphere water can be expected in the corresponding Mn^{2+} complexes. Therefore, we have also investigated ligand H_3L^3 possessing only three carboxylate functions and therefore ensuring the formation of a monohydrated Mn^{2+} complex. The thermodynamic stabilities of the Mn^{2+} complexes formed with the three ligands have been characterized and compared to the stability of Cu^{2+}, Zn^{2+}, Mg^{2+} and Ca^{2+} analogues. The dissociation kinetics of MnL^1, MnL^2 and MnL^3 has been assessed in the presence of varying concentrations of Cu^{2+}. Finally, the MnL^3 complex has been characterized with respect to its relaxation properties. The water exchange rate has been measured by variable temperature ^{17}O NMR, and ^1H NMRD profiles have been recorded and analysed to yield the parameters describing rotational dynamics. Although the kinetic inertness of these complexes is by far much lower than what was expected and prevents any *in vivo* use, their comparison reveals considerably higher inertness for the monohydrated vs. the non-hydrated analogue. It is related to different dissociation mechanism and these novel mechanistic insights could help design more inert Mn^{2+} complexes in the future.

Results and discussion

Thermodynamic stabilities

The protonation constants of the ligands L^1, L^2 and L^3, defined in Equation 1, were determined by potentiometric titration at 0.15 M NaCl ionic strength and 25 °C and are shown in Table 1.

$$K_{\mathrm{i}}^{\mathrm{H}} = \frac{[\mathrm{H_iL}]}{[\mathrm{H_{i-1}L}][\mathrm{H^+}]} \mathrm{i} = 1 - 5 \quad (1)$$

Table 1. Ligand protonation constants (25 °C, *I*=0.15M NaCl; standard deviations are given in brackets).

	L^1	L^2	L^3	EDTA[a]	OBETA[b]
$\log K_{H1}$	8.44(2)	8.47(2)	8.74(1)	9.17	9.34
$\log K_{H2}$	7.94(1)	7.79(1)	8.11(1)	5.99	8.32
$\log K_{H3}$	2.76(1)	2.73(2)	2.88(1)	2.73	3.19
$\log K_{H4}$	1.91(1)	2.77(1)	1.73(1)	2.01	2.19
$\log K_{H5}$	-	1.87(2)	1.47(2)	1.38	1.77
$\Sigma \log K_{Hi}$	21.05	23.63	22.93	21.28	23.34

a: ref. [12].b :25 °C, *I*=0.1 M KCl, ref. [18]

The first two constants correspond to the protonation of the two aliphatic amines while the last two protonations constants of L^1 and the last three protonation constants of L^2 and L^3 are attributed to acetate functions. Protonation of the pyridine nitrogen is not observed under the experimental conditions (pH=1.8-12), as it has been reported for analogous ligands.[14] The pyridine moiety decreases the basicity of the exocyclic nitrogens which results in a slightly lower value of the first protonation constant $\log K_{H1}$ for each ligand (L^1, L^2 and L^3) with respect to EDTA or OBETA. On the other hand, the second protonation constant, $\log K_{H2}$, is considerably lower for EDTA (EDTA=ethylenediamine-*N,N,N'N'*-tetraacetatic acid) due to electrostatic repulsion between the protonated nitrogen atoms in consequence of a shorter distance within the ligand backbone.

View Article Online
DOI: 10.1039/C8NJ00648B

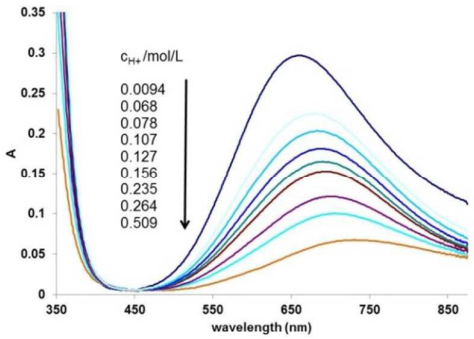

Figure 1. UV-visible spectra of recorded in a solution containing 2.5 mM Cu^{2+} and L^3 at increasing concentrations of H^+, 25 °C, 1.0 M NaCl.

The stability and the protonation constants, logK_{ML} and logK_{HML}, of the complexes formed with Mn^{2+} and other endogenous cations have been measured by potentiometric titration at *I*=0.15 M NaCl ionic strength and 25 °C (Table 2). Cu^{2+} forms very stable complexes, thus their stability constants had to be assessed by combining pH-potentiometry and UV-visible spectrophotometry. UV-visible spectra of CuL^3 as a function of the proton concentration are shown in Figure 1 (see ESI for CuL^1).

$$K_{\mathrm{ML}} = \frac{[\mathrm{ML}]}{[\mathrm{M}][\mathrm{L}]} \quad (2)$$

$$K_{H_nML} = \frac{[H_n\mathrm{ML}]}{[H_{n-1}\mathrm{ML}][\mathrm{H}^+]} \quad (3)$$

In order to confirm the equilibrium model used to analyse the potentiometric data for the MnL^3 (1:1) system, the pH-dependency of the relaxivity has been recorded and is shown in Figure 2 in comparison with the species distribution diagram (calculated from the stability and protonation constants obtained by potentiometry). The perfect match between the concentration distribution curves and the pH profiles confirms the reliability of the equilibrium model.

The stability constants obtained for MnL^1 and MnL^2 are comparable and similar to that reported for $[Mn(OBETA)]^{2-}$ (Table 2) while they are greater than the logK_{ML} value of $[Mn(EDTA)]^{2-}$ (OBETA=2,2'-oxybis(ethylamine)-N,N,N',N'-tetraacetic acid). As expected, the loss of a coordinating donor atom for L^3 results in a stability decrease of the corresponding Mn^{2+}complex as compared to MnL^1 and MnL^2. For each of the three ligands, the Cu^{2+} and Zn^{2+} complexes have higher stability constants than the Mn^{2+} analogues, following the stability order of the Irving-William's series.[19] Mg^{2+} and Ca^{2+} form complexes of relatively low stability with L^1, L^2 and L^3.

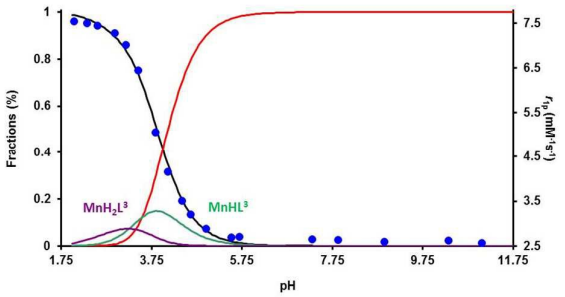

Figure 2. pH-dependent relaxivities (blue dots) measured in a solution containing equimolar quantities of Mn^{2+} and L^3 (20 MHZ, 25 °C) and species distribution curves (solid lines) calculated by using the stability constants presented in Table 2.

Table 2. Stability constants of the complexes (25 °C, *I*=0.15M NaCl; standard deviations are given in brackets) and pMn values calculated for [Mn]=10μM, [L]=10μM, pH=7.4.

		Mn^{2+}	Cu^{2+} [a]	Zn^{2+}	Mg^{2+}	Ca^{2+}
L^1	logK_{ML}	14.13(2)	17.63[b]	14.83(2)	8.44(2)	9.43[c]
	logK_{HML}	2.78(3)	3.45	3.68(1)	5.21(9)	-
	logK_{H2ML}	2.32(5)	-	2.19(1)	-	-
	pMn	8.72				
L^2	logK_{ML}	13.89(1)	15.64[c]	16.93[c]	-	9.81[c]
	log $_{HML}$	3.03(1)	3.37	3.70	-	-
	pMn	8.64				
L^3	logK_{ML}	11.97(2)	18.91(2)	15.57(2)	6.03(1)	7.27(1)
	logK_{HML}	3.54(4)	3.09(2)	2.67(2)	6.29(7)	5.94(3)
	logK_{H2ML}	3.26(8)	1.91(2)	2.03(3)	-	-
	logK_{MLOH}	12.11(2)	-	12.38(4)	-	-
	logK_{M2L}	-	-	17.87(6)	-	-
	pMn	7.42				
EDTA	logK_{ML}	12.46[d]	19.02	15.92[e]	7.61[e]	9.53[e]
	logK_{HML}	2.95	3.15	3.23	-	2.92
	pMn	7.83	2.04	1.50		
OBETA[f]	logK_{ML}	13.57	18.40	15.00	7.95	9.77
	logK_{HML}	3.45	3.71	3.18	-	-
	logK_{H2ML}	-	2.05	-	-	-
	logK_{M2L}	-	5.74	2.05	-	-
	logK_{M2LH-1}	-	6.42	-	-	-
	logK_{M2LH-2}	-	8.56	-	-	-
	pMn	7.83				
CDTA[e]	logK_{ML}	14.32	19.78	16.75	9.14	10.23
	logK_{HML}	2.90	2.91	2.57	3.53	3.58
	logK_{H2ML}	1.89	1.10	1.58		
	pMn	8.68				
PyC3A[g]	logK_{ML}	14.14				
	logK_{HML}	2.43				
	pMn	8.17				

a: from combined pH-potentometry and UV-visible spectrophotometry data; b: 25 °C, *I*=1M NaCl ref.[20]; c: 25 °C, *I*=0.1M KCl ref. [14]; d: ref [12]; e: ref[9]; f: 25 °C, *I*=0.1M KCl ref [18]; g: ref [5]

In order to directly compare the relative stability of the various Mn^{2+} complexes, the pM values referring to the concentrations of free manganese ion in solution (pMn=-log[Mn^{2+}]) were calculated for the conditions [Mn]=[L]=10 μM; pH=7.4 (Table 2). A higher pMn value refers to a higher conditional stability constant, thus a higher

View Article Online
DOI: 10.1039/C8NJ00648B

stability at the given pH; the minimal pMn value (in the absence of metal complexation) is 5. The highest pMn values are obtained for MnL^1 and MnL^2 which indicates that these complexes are expected to have the highest stability at physiological conditions. The pMn data collected in Table 3 show that L^1 and L^2 form more stable complexes with Mn^{2+} than EDTA, whereas MnL^3 has similar conditional stability to that of $[Mn(EDTA)]^{2-}$. The pMn values calculated for MnL^1 and MnL^2 are close to that of the $[Mn(CDTA)]^{2-}$ (pM=8.68)[12] or $[Mn(PyC3A)]^-$(pM=8.17)[5] which are referred to be excellent open-chain candidates for Mn^{2+} complexation. Thus L^1 and L^2 can be also regarded as good chelators for Mn^{2+} from a thermodynamic point of view.

Inertness of MnL^1, MnL^2 and MnL^3 complexes

In contrast to Gd^{3+}, Mn^{2+} has an endogenous elimination pathway *via* the hepatobiliary system. Nevertheless, given the high contrast agent concentrations used in MRI, Mn^{2+} complexes are also required to possess sufficient kinetic inertness in order to avoid release of substantial amounts free metal ion which could lead to acute manganese toxicity. In order to assess the kinetic inertness of our complexes, their dissociation was studied in transmetallation reactions in the presence of Cu^{2+}. Given the low molar UV-Vis absorption of Mn^{2+} complexes, the transmetallation reaction can be followed either *via* the relaxivity increase that results from Mn^{2+} release or *via* the increase in UV-Vis absorbance due to the formation of the Cu^{2+} complex. The transmetallation of our Mn^{2+} complexes with Cu^{2+} was too fast to be monitored by classical spectrophotometry, thus a "stopped-flow" method was used at different pHs and in the presence of 10-40 fold Cu^{2+}excess in order to ensure pseudo-first order conditions. We should note that this spectrophotometric stopped-flow technique would not be adapted to follow the transmetallation with Zn^{2+}, as the UV-Vis spectra of the Zn^{2+} complexes is expected to be similar to that of the Mn^{2+} analogues.

The reaction rate of the transmetallation can be expressed as in Equation 4, where k_{obs} corresponds to the pseudo-first order rate constant and $[MnL]_{tot}$ is the total MnL concentration.

$$\frac{-d[MnL]_{tot}}{dt} = k_{obs}[MnL]_{tot} \quad (4)$$

The dissociation rate constants (k_{obs}) observed in the pH range 3.2–5.0 and in the presence of 10–40-fold excess of Cu^{2+} are depicted in Figure 3 for the three MnL complexes.

MnL^1 and MnL^2 have similar behavior. They show an increase of the observed dissociation rate constants with increasing Cu^{2+} concentration and with decreasing proton concentration (for any Cu^{2+} concentration). MnL^3 behaves very differently. For this complex, the pseudo-first order rate constants increase with increasing acidity while they are little affected by the concentration of the exchanging Cu^{2+}. This evidences that the different possible pathways contribute differently to the dissociation of MnL^1 and MnL^2 as compared to MnL^3. For MnL^1 and MnL^2, the copper-assisted dissociation is the predominant mechanism, as shown by

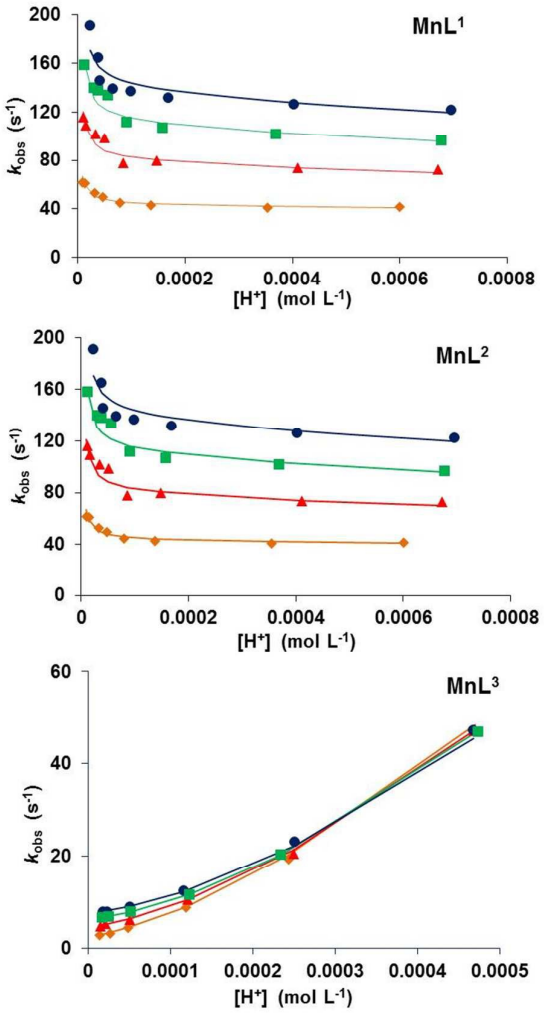

Figure 3. Dependence of the pseudo-first order rate constants, k_{obs}, on the concentration of H^+ and Cu^{2+} for the transmetallation of MnL complexes. The Cu^{2+} excess was 10 (♦), 20 (▲), 30 (■) and 40 (●) fold. The curves represent the fit as described in the text.

the strong dependency of k_{obs} on the Cu^{2+} concentration. The increase of the dissociation rate constants with increasing pH is the consequence of the presence of $Cu(OH)^+$ which is known to attack Mn^{2+} complexes more efficiently than the non-hydrolized Cu^{2+} ion itself, a phenomenon already reported in literature examples.[21] The greater reaction efficiency of $Cu(OH)^+$ is due to the formation of hydrogen bonds or hydroxide bridges which stabilize the

DOI: 10.1039/C8NJ00648B

intermediate formed. In the case of MnL^3, the strong increase of the rate constants with increasing proton concentration evidences the predominant role of the proton-catalyzed pathway while the Cu^{2+}-assisted dissociation pathway has much less importance, as shown by the limited effect of copper concentration on k_{obs}. This difference between MnL^1, MnL^2 *vs* MnL^3 can be rationalized by the different number of donor atoms of the ligands. L^3 has one less coordinating functions which restricts Cu^{2+} binding to the MnL complex thus the formation of reactive dinuclear intermediates and limits the importance of the metal-assisted dissociation pathway. These observations also help understand the origin of the high kinetic lability of $[Mn(DTPA)]^{3-}$ evidenced in the literature.[22] If we consider that Mn^{2+} is heptacoordinated in $[Mn(DTPA)]^{3-}$, one donor atom remains available for protonation (which enhances proton assisted dissociation) or for dinuclear complex formation (formation of the critical dinuclear intermediate). Both of these features contribute to an increased lability of the complex. In fact, structural data available for a DTPA-bisamide derived from 4-aminobenzoic amine indicate a heptacoordinated distorted pentagonal bipyramid polyhedron around the Mn^{2+} ion in which one of Mn–N (terminal) bond is elongated (2.569 Å vs. 2.379 Å and 2.390 Å) and the carboxylate group attached to this N atom remains uncoordinated.[23]

By taking into account the proton- and metal-assisted pathways and the presence of differently protonated species in the pH-region of the experiments, the general dissociation mechanism of Mn^{2+} complexes can be presented as in Scheme 2.

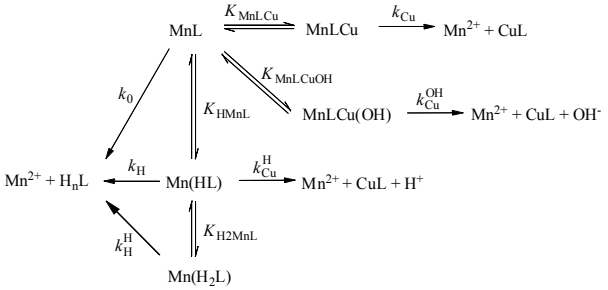

Scheme 2. Reaction pathways for the dissociation of MnL complexes

By considering the different pathways depicted in Scheme 2, the pseudo-first-order rate constant, k_{obs}, can be expressed as in Equation 5:

$$k_{obs} = \frac{k_0 + k_1[H^+] + k_2[H^+]^2 + k_3[Cu^{2+}] + k_4[Cu^{2+}][H^+] + k_5[Cu^{2+}][OH^-]}{1 + K_{HMnL}[H^+] + K_{HMnL}K_{H2MnL}[H^+]^2 + K_{MnLCu}[Cu^{2+}]} \quad (5)$$

where $K_{HMnL}=[HMnL]/[MnL][H^+]$, $K_{H2MnL}=[H_2MnL]/[HMnL][H^+]$, $K_{MnLCu}=[MnLCu]/[MnL][Cu]$, $K_{CuOH}=[Cu(OH)^+][H^+]/[Cu]$, $k_1=k_H \cdot K_{HMnL}$, $k_2=k_H^H \cdot K_{HMnL} \cdot K_{H2MnL}$, $k_3=k_{Cu} \cdot K_{MnLCu}$, $k_4= k_{Cu}^H \cdot K_{HMnL}$ and $k_5= k_{Cu}^{OH} \cdot K_{CuOH}$).

The observed rate constants for MnL^1, MnL^2 and MnL^3 were fitted to Equation 5. In the fit, the protonation constants were fixed to the values determined by potentiometry (Table 2). We have considered all possible dissociation pathways; however, the fit of the k_{obs} values clearly confirmed that several terms can be neglected in the overall expression of k_{obs} (Equation 5), which is in full accordance with the qualitative observations discussed above. Namely, spontaneous dissociation appears to be negligible for each of the three complexes, as small negative values with large errors have been obtained for k_0 characterizing this pathway. For MnL^1 and MnL^2, in the absence of pH dependency of k_{obs} in acidic solutions, it was not possible to determine the rate constants characterizing the proton-assisted dissociation (k_1 or k_2). The dissociation occurs mainly *via* the direct attack of the exchanging metal ion on MnL, characterized by k_3. The metal-assisted dissociation of the protonated HMnL complexes, characterized by k_4, has no importance for any of the three systems. Finally, for MnL^1 and MnL^2, the pathway which involves the attack of the hydroxo-complex $Cu(OH)^+$ contributes also to dissociation at higher pHs, as evidenced by the importance of the term characterized by the k_5 constant. The best-fit parameters calculated are listed in Table 3.

The existence of various dissociation pathways characterized by their corresponding rate constants makes the comparison of the kinetic inertness of different Mn^{2+} complexes difficult. Therefore, the dissociation half-lives ($t_{1/2}$) were calculated for physiological conditions (pH=7.4 and $c_{Cu2+}=1\times10^{-5}$ M concentration of the exchanging Cu^{2+} ion; Table 3). The data clearly show that the kinetic inertness of these MnL complexes is lower than that of $[Mn(EDTA)]^{2-}$, mainly due to the several orders of magnitude higher efficiency of the copper-assisted dissociation pathway. These complexes are expected to dissociate in biological medium and their *in vivo* use cannot be envisaged. It must be noted that for MnL^1 and MnL^2 the half-lives were calculated by considering solely the metal-catalyzed dissociation pathway since no data could be obtained for the acid-catalyzed dissociation.

Table 3. Rate constants characterizing the dissociation of MnL complexes (25 °C).

	L^1	L^2	L^3	EDTA[b]	CDTA[b]
k_1 /$M^{-1}s^{-1}$	-	-	$(3.1\pm0.3)\times10^4$	5.2×10^2	4.0×10^2
k_2 /$M^{-2}s^{-1}$	-	-	$(5.6\pm0.2)\times10^8$	2.3×10^8	
k_3 /$M^{-1}s^{-1}$	$(1.45\pm0.04)\times10^4$	$(1.7\pm0.1)\times10^4$	$(1.13\pm0.05)\times10^3$	45	
k_5 /$M^{-2}s^{-1}$	$(1.17\pm0.07)\times10^{13}$	$(3.3\pm0.5)\times10^{10}$		-	
K_{MnLCu}	45±5	20±10	41±6		79
$t_{1/2}$[a] (s)	0.024	2.75	55	274	4.3×10^4

a: calculated for pH=7.4 and $[Cu^{2+}]=1\times10^{-5}$M, b: ref[12]

Despite the disappointing kinetic inertness of these pyridine-based complexes, the results bring valuable insights into the dissociation mechanism of Mn^{2+} chelates. They evidence that a minor variation

View Article Online
DOI: 10.1039/C8NJ00648B

in the ligand structure might have dramatic consequences on the relative importance of the metal- *vs*. proton-assisted pathways. Interestingly, a higher number of donor atoms (L^1 and L^2) can lead to a higher thermodynamic stability but to a lower kinetic inertness as the attack of the exchanging metal ion (Cu^{2+} or its hydroxo-complex) is facilitated when more coordinating functions are available.

Relaxometric properties

Proton relaxivity, r_{1p}, is defined as the enhancement of the longitudinal water proton relaxation rate in the presence of 1 mM concentration of a paramagnetic agent and it is a direct measure of MRI contrast agent efficiency. It is directly proportional to the number of hydration water molecules of the complex, and also dependent on other microscopic factors, such as the exchange rate of the inner sphere water, the rotational dynamics of the complex and the electron spin relaxation times. The proton relaxivities measured at 25 °C and 20 MHz for MnL^2 and MnL^3 are 1.51 $mM^{-1}s^{-1}$ and 2.64 $mM^{-1}s^{-1}$, respectively, corresponding to typical values for non-hydrated and monohydrated Mn^{2+} complexes, as expected from the ligand structure. In order to fully describe the parameters that govern relaxation behaviour of the monohydrated MnL^3, relaxivities were measured in a large magnetic field range (0.01-400 MHz) and at two temperatures (25 and 37 °C). These Nuclear Magnetic Relaxation Dispersion (NMRD) profiles have been complemented by variable temperature ^{17}O transverse relaxation rate and chemical shift measurements which allow, respectively, direct assessment of the water exchange rate and estimation of the hydration number.

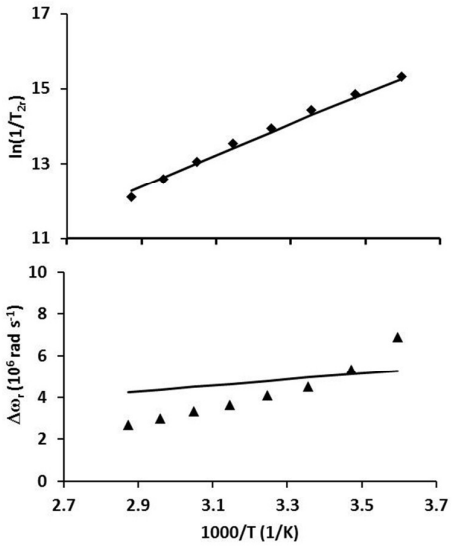

Figure 4. Variable temperature, reduced transverse ^{17}O relaxation rates ($1/T_{2r}$) (top) and reduced chemical shifts ($\Delta\omega_r$) (bottom) for MnL^3. The curves represent the fit as described in the text.

The variable-temperature transverse ^{17}O relaxation times and chemical shifts of a MnL^3 solution recorded at 9.4 T are presented in Figure 4. Based on the ligand structure, one can assume hexadentate coordination with one inner-sphere water molecule in the complex. The ^{17}O chemical shifts measured are in accordance with this hypothesis; the scalar coupling constant fitted is $A_O/\hbar$ = -40×10^6 rad s^{-1}, typical of a Mn^{2+} complex (Figure 4). We note the relatively bad quality of the fit of the chemical shifts; however, one should be aware of the difficulties associated with determining the chemical shift for the very broad water ^{17}O NMR peaks of strongly relaxing paramagnetic samples such as Mn^{2+} complexes.

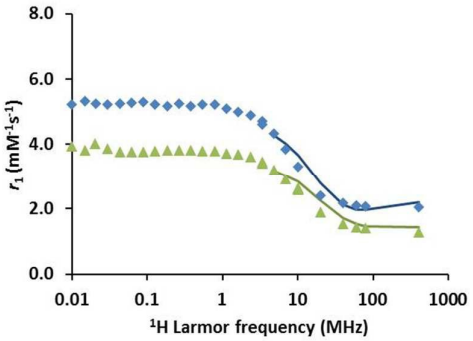

Figure 5. Variable field ^1H relaxivities of MnL^3 at 37 °C (▲) and 25 °C (♦). The curves represent the fit as described in the text.

The temperature dependence of the transverse ^{17}O relaxation rates of MnL^3 indicates a fast exchange regime ($1/T_2$ increases with decreasing temperature)**.** The reduced transverse ^{17}O relaxation rates and chemical shifts were fitted according to the Solomon-Bloembergen-Morgan theory of paramagnetic relaxation to obtain the water exchange rate, k_{ex}^{298}, the activation enthalpy, $\Delta H^{\neq}$, and entropy, $\Delta S^{\neq}$, and scalar coupling constant, A/ħ. The electron spin relaxation has been described by a simple exponential function. The water exchange rate is extremely high and the fit of the ^{17}O $\ln(1/T_{2r})$ data does not allow for calculating the parameters describing electron spin relaxation. Indeed, by fixing $1/T_{1e}^{298}$ to values between 5×10^5 s^{-1} and 1×10^8 s^{-1} and its activation energy, E_{T1e} to 1 kJ/mol, the calculated value of k_{ex}^{298} was invariably 2.8×10^9 s^{-1}. The equations used are given in the ESI and the parameters obtained are shown in Table 4.

Table 4. Parameters characterizing water exchange and scalar coupling constants obtained from ^{17}O NMR data for MnL complexes

	q	k_{ex}^{298} /10^{6}s^{-1}	$\Delta H^{\neq}$ /kJ.mol^{-1}	$\Delta S^{\neq}$ /J.mol^{-1}K^{-1}	$A_0/\hbar$ /10^{6}rads^{-1}
MnL^3	1	2800±600	34±5	51±15	-(40±5)
$[Mn(CDTA)]^{2-}$ [a]	1	140	42.5	-	-26.4
[Mn(1,4-DO2A)][b]	0.87	1134	29.4	-	-43

View Article Online
DOI: 10.1039/C8NJ00648B
Journal Name ARTICLE

$[Mn_2(ENOTA)]^c$	1	5.5	20.5	-28	-32.7
$[Mn(H_2O)_6]^{2-d}$	6	2.1	32.9	+5.7	-33.3

a: ref [24]; b: ref [25]; c: ENOTA: see ESI for structure, ref [26]; d: ref [27]

This water exchange rate is among the highest values reported for a Mn^{2+} complex; it is comparable to that of $[Mn(NTA)(H_2O)_2]^-$ (k_{ex}^{298}=1.5×10^9 s^{-1}),[28] or $[Mn(1,4\text{-}DO2A)(H_2O)_{0.87}]$ (k_{ex}^{298}=1.1×10^9 s^{-1})[25] (H_3NTA = nitrilotriacetatic acid; H_2(1,4-DO2A) = 1,4,7,10-tetraazacyclododecane-1,4-diacetic acid). The activation entropy, $\Delta S^{\neq}$, has a high positive value, suggesting dissociative water exchange mechanism, even if the unambiguous attribution of the mechanism would require variable pressure ^{17}O T_2 data. The dissociative mechanism implies the leaving of the outgoing water molecule before the entering of a new water molecule to form a six-coordinate transition state. A dissociatively activated mechanism can be indeed expected considering the seven-coordinate structure of the complex and the fact that in poly(amino carboxylate) chelates, the Mn^{2+} ion is typically in six- or seven-coordinate environments.

The NMRD curves reflect the magnetic field dependency of the proton relaxivity and are useful to distinguish between different relaxation mechanisms for a paramagnetic complex. The profiles have a form typical of low molecular weight chelates with a single dispersion between 1 and 10 MHz. They have been analysed according to the Solomon-Bloembergen-Morgan framework (see ESI for the equations) between 6 and 400 MHz, where the validity of the theory holds for small complexes. In this fit, the water exchange parameters were fixed to the values determined above. The distances between the Mn^{2+} ion and the protons in the inner and outer coordination sphere were fixed to typical values, r_{MnH}=2.83 Å and a_{MnH}=3.6 Å, respectively, and the diffusion coefficient and its activation energy to D_{MnH}^{298}=26×10^{-10} m^{2}s^{-1} and E_{DMnH}=20 kJmol^{-1}.[25] The rotational correlation time, τ_R^{298}, its activation energy, E_R, and the parameters referring to electron spin relaxation, Δ^2 and τ_v^{298}, have been calculated in the fit; they are shown in Table 5. The value of the rotational correlation time is in the range expected for such a small molecule and comparable to those of similar Mn^{2+} chelates.

Table 5. Parameters obtained from the fit of ^{1}H NMRD data for different MnL complexes

	τ_R^{298}/ps	E_R/kJ.mol^{-1}	τ_v^{298}/ps	Δ^2/10^{20} s^{-1}
MnL^3	25±5	20±3	2±1	15±1
$[Mn(1,4\text{-}DO2A)]^a$	46	19.1	4.4	0.48
$[Mn_2(ENOTA)]^b$	25.5	18	7.7	4.7

a: ref. [25]; b: ref [26]

Conclusions

The inclusion of structural motifs that induce rigidity into the skeleton of poly(amino carboxylate) ligands is expected to yield in increased kinetic inertness of their metal complexes. In this context, we have studied the Mn^{2+} chelates of three, pyridine-containing linear ligands. Although their thermodynamic stabilities are higher (L^1 and L^2) or comparable (L^3) to that of $[Mn(EDTA)]^{2-}$, the kinetic inertness of these Mn^{2+} complexes and in particular of MnL^1 and MnL^2 is unexpectedly low, mainly due to very efficient dissociation pathways mediated by the attack of Cu^{2+} or the hydroxo complex $Cu(OH)^+$. Interestingly, the ligand L^3 providing one less carboxylate donor function ensures higher kinetic inertness for the Mn^{2+} chelate, as it is less prone to metal-assisted dissociation. The MnL^3 complex is monohydrated and has very fast water exchange.

Experimental

The synthesis of ligands H_4L^1, H_4L^2 and H_3L^3 was previously described.[14, 29] The ligand concentrations were determined by adding an excess of lanthanide solution to the ligand solution and titrating the metal excess with standardized Na_2H_2EDTA in urotropine buffer (pH 5.6–5.8) in the presence of xylenol orange as an indicator. The concentration of the metal solutions was determined similarly by complexometric titrations. Samples of MnL^1, MnL^2 and MnL^3 complexes for the dissociation kinetic studies and of MnL^3 for the ^{17}O NMR and NMRD measurements have been prepared by mixing equimolar amounts of $MnCl_2$ and ligand solutions and adjusting the pH to 6.5 with a NaOH solution.

Potentiometry

Potentiometric titrations were performed to determine protonation constants of the ligands and stability constants of the complexes at 1:1 and 2:1 metal to ligand ratios. Samples were thermostated at 25 °C under constant nitrogen flow to provide inert atmosphere. Titrations were performed at 0.15 M NaCl ionic strength with a ~0.2 M NaOH solution and the ligand concentration in the titrated solutions (in 6 mL total volume) was ~2 mM. Titrations were done in the pH range 1.8-11.8 or until metal hydroxide precipitation occurred (in samples with metal excess). Extra volume of HCl was added to the starting solution to obtain a starting pH of 1.8. pH-potentiometric titrations were performed with a Metrohm 888 Titrando automatic titration system and a Metrohm combined electrode. H^+ ion concentrations were obtained from the measured pH using the method proposed by Irving et al.[30] PESQUAD program was used for the calculation of the equilibrium constants.[31]

UV-visible spectroscopy

To determine the stability constants of the Cu^{2+} complexes, UV-visible absorption spectra were recorded on a Varian Cary 1E UV-visible spectrophotometer (L^2) or a PerkinElmer Lambda

View Article Online
DOI: 10.1039/C8NJ00648B

19 spectrometer (L^3) in the region λ=350-875 nm at 25 °C. Out-off-cell samples were prepared containing Cu^{2+} (2.5 mM), slight excess of the ligand, 1 M NaCl and different (5-500 mM) HCl. The samples were equilibrated few days before the measurements.

For the dissociation kinetic experiments, the rates of the metal exchange reactions were too fast to be followed using a standard UV-spectrometric method. The dissociation of the Mn^{2+} complexes was therefore investigated with a stopped-flow technique (Applied Photophysics DX-17MV). The reactions were followed at 300 nm in the pH range 3.4-4.9 by using *N,N'*-dimethylpiperazine (DMP, 20 mM) buffer. The concentration of the complexes was 0.5 mM, while the Cu^{2+} concentration was 10-40 times higher to ensure pseudo-first-order conditions. The temperature was maintained at 25 °C and the ionic strength was kept constant (0.15 M NaCl). The pseudo-first-order rate constants (k_{obs}) were calculated by fitting the absorbance-time data to the following equation:

$$A_t = (A_0 - A_e)e^{-k_{obs}\,t} + A_e \quad (6)$$

A_t, A_0 and A_e are the absorbance at time t, at the start and at equilibrium, respectively. The calculations were performed with the computer program Scientist, by using a standard least-squares procedure.

Relaxometric measurements

^{1}H relaxometric measurements were performed using a Bruker Minispec MQ-20 NMR analyzer at 20 MHz and 25 °C. The temperature of the sample holder was set (25.0±0.2 °C) and controlled with the use of a circulating water bath. The longitudinal relaxation times (T_1) were measured by using the inversion recovery method by averaging 5-6 data points obtained at 14 different τ values. The relaxivities of the complexes were determined according to a methodology slightly different from the standard procedure (by plotting the reciprocal longitudinal relaxation times of the complexes against their concentrations). Batch samples were prepared under argon atmosphere at 2.0 mM ligand concentration (the pH in these samples was kept constant at pH=6.70 with the use of HEPES buffer (*I*=0.15 M NaCl, 25 °C)). Various amounts of $MnCl_2$ were added to these solutions and longitudinal relaxation times were measured. Because under these conditions only one Mn^{2+} ion containing species is present in solution in each system (complexes of MnL composition), the curve obtained by plotting $1/T_{1p}$ for the samples with [L]>[Mn^{2+}] as a function of Mn^{2+} concentration gives a straight line, with a slope that is equal to the relaxivity of the complex. Stability constants of Mn^{2+} complexes were also probed by using ^{1}H relaxometry. The T_1 longitudinal relaxation time of water protons was measured at 20 MHz for different batch samples containing equimolar amounts of Mn^{2+} and H_4L^2 or H_3L^3 at 0.15 M NaCl and various amounts of acid were added to cover the pH range of 1.75-10.96 for MnL^2 and 2.03-11.06 for MnL^3.

^{1}H NMRD profiles of an aqueous MnL^3 solution (1.87 mM, pH 7.2) were measured at 25 and 37 °C on a Stelar SMARTracer Fast Field Cycling NMR relaxometer (0.00024–0.24 T, 0.01–10 MHz ^{1}H Larmor frequency) and a Bruker WP80 NMR electromagnet adapted to variable-field measurements (0.47–1.88 T, 20–80 MHz), and controlled by the SMARTracer PC-NMR console. The temperature was controlled by a VTC91 temperature control unit and maintained by a gas flow. The temperature was determined according to previous calibration with a Pt resistance temperature probe. The relaxivities at 400 MHz were obtained on a Bruker Advanced 400 MHz spectrometer using a 5mm BBFO probe.

^{17}O NMR

Variable-temperature ^{17}O NMR measurements of aqueous solutions of MnL^3 (3.78 mmol kg^{-1}, pH 7.2 (T_2 measurements) and 37.91 mmol kg^{-1}, pH 7.7 (shift measurements)) were performed on a Bruker Advanced 400 MHz spectrometer using a 10 mm BBFO probe (9.4 T, 54.2 MHz) in the temperature range 1–75 °C. The temperature was calculated according to published calibration routines with ethylene glycol and MeOH.[32] The corresponding ZnL^3 complex at identical concentration and pH was used as diamagnetic reference. Transverse ^{17}O relaxation times were obtained by the Carl-Purcell-Meiboom-Gill spin-echo technique.[33] To eliminate susceptibility corrections to the chemical shifts,[34] the sample was placed in a glass sphere fixed in a 10 mm NMR tube. To improve sensitivity, $H_2{}^{17}O$ (10 % $H_2{}^{17}O$, CortecNet) was added to achieve ~1% ^{17}O content in the sample.

Conflicts of interest

There are no conflicts to declare.

Acknowledgements

We acknowledge support of the Ligue contre le cancer and the PHC program Balaton (France). Authors are grateful for the support granted by the Hungarian National Research, Development and Innovation Office (NKFIH K-120224 project) and for the János Bolyai Research Scholarship of the Hungarian Academy of Sciences (Gy.T. and K.F.K.). The research was also supported by the EU and co-financed by the European Regional Development Fund under the projectsGINOP-2.3.2-15-2016-00008 and GINOP-2.3.3-15-2016-00004. This work was carried out within the frame of the COST CA15209 Action "European Network on NMR Relaxometry".

References

1. A. Merbach, L. Helm and E. Toth, *The Chemistry of Contrast Agents in Medical Magnetic resonance Imaging*, Second Edition edn., John Wiley & Sons, Chichester, 2013.
2. T. Grobner, *Nephrology Dialysis Transplantation*, 2006, **21**, 1104-1108.
3. E. Kanal and M. F. Tweedle, *Radiology*, 2015, **275**, 630-634.

View Article Online
DOI: 10.1039/C8NJ00648B

4. B. Drahos, I. Lukes and E. Toth, *Eur. J. Inorg. Chem.*, 2012, 1975-1986.
5. E. M. Gale, I. P. Atanasova, F. Blasi, I. Ay and P. Caravan, *J. Am. Chem. Soc.*, 2015, **137**, 15548-15557.
6. J. Zhu, E. M. Gale, I. Atanasova, T. A. Rietz and P. Caravan, *Chem. Eur. J.*, 2014, **20**, 14507-14513.
7. R. Artali, Z. Baranyai, M. Botta, G. B. Giovenzana, A. Maspero, R. Negri, G. Palmisano, M. Sisti and S. Tollari, *New J. Chem.*, 2015, **39**, 539-547.
8. E. Molnar, N. Camus, V. Patinec, G. A. Rolla, M. Botta, G. Tircso, F. K. Kalman, T. Fodor, R. Tripier and C. Platas-Iglesias, *Inorg. Chem.*, 2014, **53**, 5136-5149.
9. C. Vanasschen, E. Molnar, G. Tircso, F. K. Kalman, E. Toth, M. Brandt, H. H. Coenen and B. Neumaier, *Inorg. Chem.*, 2017, **56**, 7746-7760.
10. B. Drahos, V. Kubicek, C. S. Bonnet, P. Hermann, I. Lukes and E. Toth, *Dalton Trans.*, 2011, **40**, 1945-1951.
11. G. Anderegg, *Helv. Chim. Acta*, 1964, **47**, 1801-&.
12. F. K. Kalman and G. Tircso, *Inorg. Chem.*, 2012, **51**, 10065-10067.
13. L. Pellegatti, J. Zhang, B. Drahos, S. Villette, F. Suzenet, G. Guillaumet, S. Petoud and E. Toth, *Chem. Commun.*, 2008, 6591-6593.
14. C. S. Bonnet, F. Buron, F. Caille, C. M. Shade, B. Drahos, L. Pellegatti, J. Zhang, S. Villette, L. Helm, C. Pichon, F. Suzenet, S. Petoud and E. Toth, *Chem. Eur. J.*, 2012, **18**, 1419-1431.
15. F. Caille, C. S. Bonnet, F. Buron, S. Villette, L. Helm, S. Petoud, F. Suzenet and E. Toth, *Inorg. Chem.*, 2012, **51**, 2522-2532.
16. H. Su, C. Wu, J. Zhu, T. Miao, D. Wang, C. Xia, X. Zhao, Q. Gong, B. Song and H. Ai, *Dalton Trans.*, 2012, **41**, 14480-14483.
17. C. Wu, D. Li, L. Yang, B. Lin, H. Zhang, Y. Xu, Z. Cheng, C. Xia, Q. Gong, B. Song and H. Ai, *J. Mater. Chem. B*, 2015, **3**, 1470-1473.
18. R. Negri, Z. Baranyai, L. Tei, G. B. Giovenzana, C. Platas-Iglesias, A. C. Benyei, J. Bodnar, A. Vagner and M. Botta, *Inorg. Chem.*, 2014, **53**, 12499-12511.
19. H. Irving and R. J. P. Williams, *J. Chem. Soc.*, 1953, 3192-3210.
20. C. S. Bonnet, S. Laine, F. Buron, G. Tircso, A. Pallier, L. Helm, F. Suzenet and E. Toth, *Inorg. Chem.*, 2015, **54**, 5991-6003.
21. D. W. Margerum, B. A. Zabin and D. L. Janes, *Inorg. Chem.*, 1966, **5**, 250-&.
22. B. Gallez, C. Baudelet and M. Geurts, *Magn. Res. Imag.*, 1998, **16**, 1211-1215.
23. L. Ying-Chun, Z. Jing, L. Quan, M. Shu-Lan, X. Miao-Qiong and Z. Wen-Xiang, *Chinese J. Chem.*, 2005, **23**, 1012-1016.
24. J. Maigut, R. Meier, A. Zahl and R. van Eldik, *Inorg. Chem.*, 2008, **47**, 5702-5719.
25. G. A. Rolla, C. Platas-Iglesias, M. Botta, L. Tei and L. Helm, *Inorg. Chem.*, 2013, **52**, 3268-3279.
26. E. Balogh, Z. He, W. Hsieh, S. Liu and E. Toth, *Inorg. Chem.*, 2007, **46**, 238-250.
27. Y. Ducommun, K. E. Newman and A. E. Merbach, *Inorg. Chem.*, 1980, **19**, 3696-3703.
28. M. S. Zetter, E. J. Wood, J. P. Hunt, H. W. Dodgen and M. W. Grant, *Inorg. Chem.*, 1972, **11**, 2701-&.
29. C. S. Bonnet, F. Caille, A. Pallier, J. F. Morfin, S. Petoud, F. Suzenet and E. Toth, *Chem. Eur. J.*, 2014, **20**, 10959-10969.
30. H. M. Irving, M. G. Miles and L. D. Pettit, *Anal. Chim. Acta*, 1967, **38**, 475-&.
31. L. Zékany and I. Nagypal, in *Computational Methods for the Determination of Formation Constants*, ed. D. J. Leggett, Plenum Press, New York, Editon edn., 1985, p. 291.
32. D. S. Raiford, C. L. Fisk and E. D. Becker, *Anal. Chem.*, 1979, **51**, 2050-2051.
33. S. Meiboom and D. Gill, *Rev. Sci. Instrum.*, 1958, **29**, 688-691.
34. A. D. Hugi, L. Helm and A. E. Merbach, *Helv. Chim. Acta*, 1985, **68**, 508-521.

View Article Online
DOI: 10.1039/C8NJ00648B

TOC

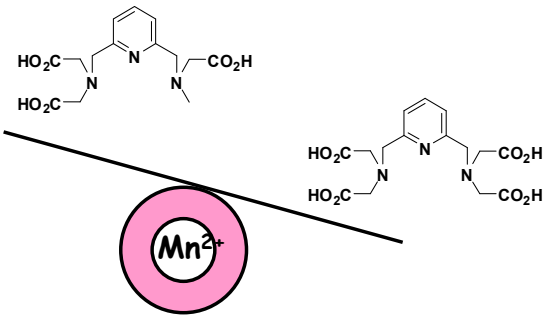

Stability, inertness and relaxometry

The loss of a coordinating donor atom in the ligand leads to lower thermodynamic stability, but higher kinetic inertness of the Mn^{2+} complex.